



Fast diffusion of silver in TiO₂ nanotube arrays

Wanggang Zhang^{1,2,3}, Yiming Liu^{1,2}, Diaoyu Zhou^{1,2}, Hui Wang^{1,2}, Wei Liang^{*1,2} and Fuqian Yang^{*3}

Full Research Paper

[Open Access](#)**Address:**

¹College of Materials Science and Engineering, Taiyuan University of Technology, Taiyuan Shanxi 030024, China, ²Key Laboratory of Interface Science and Engineering in Advanced Materials, Taiyuan University of Technology, Ministry of Education, Taiyuan Shanxi 030024, China and ³Department of Chemical and Materials Engineering, University of Kentucky, Lexington, KY 40506, USA

Email:

Wei Liang^{*} - liangwei@tyut.edu.cn; Fuqian Yang^{*} - fyang2@uky.edu

^{*} Corresponding author

Keywords:

activation energy; fast diffusion; magnetron sputtering; silver; TiO₂ nanotube

Beilstein J. Nanotechnol. **2016**, *7*, 1129–1140.

doi:10.3762/bjnano.7.105

Received: 02 May 2016

Accepted: 15 July 2016

Published: 03 August 2016

Associate Editor: R. Xu

© 2016 Zhang et al.; licensee Beilstein-Institut.

License and terms: see end of document.

Abstract

Using magnetron sputtering and heat treatment, Ag@TiO₂ nanotubes are prepared. The effects of heat-treatment temperature and heating time on the evolution of Ag nanofilms on the surface of TiO₂ nanotubes and microstructure of Ag nanofilms are investigated by X-ray diffraction, field emission scanning electron microscopy, and transmission electron microscopy. Ag atoms migrate mainly on the outmost surface of the TiO₂ nanotubes, and fast diffusion of Ag atoms is observed. The diffusivity for the diffusion of Ag atoms on the outmost surface of the TiO₂ nanotubes at 400 °C is 6.87×10^{-18} m²/s, which is three orders of magnitude larger than the diffusivities for the diffusion of Ag through amorphous TiO₂ films. The activation energy for the diffusion of Ag atoms on the outmost surface of the TiO₂ nanotubes in the temperature range of 300 to 500 °C is 157 kJ/mol, which is less than that for the lattice diffusion of Ag and larger than that for the grain boundary diffusion. The diffusion of Ag atoms leads to the formation of Ag nanocrystals on the outmost surface of TiO₂ nanotubes. Probably there are hardly any Ag nanocrystals formed inside the TiO₂ nanotubes through the migration of Ag.

Introduction

Titanium dioxide (TiO₂) has gained great attention for various applications, such as energy storage [1-8] and photo-assisted reactions [9-14], due to its inherent semiconducting characteristics, chemical stability, high photo-conversion efficiency, non-toxicity and low cost [15,16]. TiO₂ of low-dimensional structures, including nanotubes, nanoparticles, nanorods, meso-

porous spheres, nanosheets, nanowires have been synthesized via anodic oxidation, template, and hydrothermal processing to increase the ratio of surface area to volume for the maximization of effective surface area [17]. Among the low-dimensional structures, TiO₂ nanotubes (TNT) seem to be an ideal candidate for the applications in energy storage and photovoltaics.

The intrinsic poor electric conductivity and large bandgaps (approx. 3.4 eV for anatase TiO_2 [18] and approx. 3.0 eV for rutile TiO_2 [19,20]) have limited the applications of TiO_2 of low-dimensional structures. To increase the electric performance of TiO_2 , TiO_2 -based materials have been developed by incorporating metal nanoparticles in TiO_2 nanotube arrays, using electrochemical deposition [21], irradiation of microwave [22], reduction [23], and sol–gel process [24], which involve the use of aqueous solutions. In addition, the technique of magnetron sputtering has been used to deposit Ag nanostructures on the surface of TiO_2 nanotube arrays. It is worth mentioning that Enachi et al. [25] heat-treated the TiO_2 nanotube arrays after the deposition of Ag film of 50 nm on the top surface of TiO_2 nanotube arrays and observed the formation of Ag nanodots on the top surface of the TiO_2 nanotube arrays. However, they did not examine and discuss whether there exist Ag nanodots inside the TiO_2 nanotubes or on the surface of the TiO_2 nanotubes.

The microstructures of TiO_2 -based materials depend on the migration of atoms (dopants), which determine the functionality of TiO_2 -based materials. Although recent success in improving the photocatalytic activity and energy storage of Li ions in TiO_2 -based materials has been reported [26–29], the understanding of the migration of atoms (dopants) in TiO_2 nanotube arrays, which determines the evolution of the microstructures of the TiO_2 -based materials, remains elusive. In this work, we report the discovery of the fast diffusion of silver through TiO_2 nanotube arrays in forming Ag@TiO_2 nanotube arrays. The Ag@TiO_2 nanotube arrays are prepared by the heat treatment of TiO_2 nanotube arrays coated with Ag nanofilms. The microstructures of the Ag@TiO_2 nanotube arrays are characterized to determine the diffusivity and activation energy of the Ag diffusion on the surface of the TiO_2 nanotubes.

Results

The preparation route of the Ag@TiO_2 nanotubes is schematically illustrated in Figure 1. The pure TiO_2 nanotubes are prepared by a simple two-step anodization process, and then a layer of Ag film is deposited on the top of the TiO_2 nanotubes

via sputtering magnetron. The heat treatment of the TiO_2 nanotubes with Ag nanofilm leads to the formation of Ag@TiO_2 nanotubes.

Figure 2 shows typical SEM images of the pure TiO_2 nanotube arrays prepared by a two-step anodization process without heat treatment. It is evident that the prepared pure TiO_2 nanotube arrays consist of regular tubes with a diameter of 75 ± 5 nm, a wall thickness of 7 ± 2 nm and an average length of about 6.5 μm . The outmost surface of the pure TiO_2 nanotubes prepared by the two-step anodization process is relatively clean and smooth, as shown in Figure 2b. For comparison, typical SEM images of the pure TiO_2 nanotube arrays prepared by a one-step anodization process are shown in Figure S1c in Supporting Information File 1. The outmost surface of the pure TiO_2 nanotubes prepared by the two-step anodization process is much cleaner and smoother than those prepared by the one-step anodization process. No “bamboo-like” structures are present on the outmost surface of the pure TiO_2 nanotubes. Only the pure TiO_2 nanotubes prepared by the two-step anodization process were used in this work. The inserted image in Figure 2b shows the topology of the Ti surface after the nanotubes formed by the one-step anodization were ultrasonically removed. There are no TiO_2 nanotubes observable, and well-ordered round imprints are observed on the surface of the Ti foil.

The SEM image of Figure 2d reveals the closed honeycomb-like structure of the bottom surface of the pure TiO_2 nanotube arrays, similar to the structure prepared by the one-step anodization process (see Figure S1d in Supporting Information File 1). The prepared pure TiO_2 nanotube arrays exhibit a highly ordered structure, and the TiO_2 nanotubes are normal to the surface of the corresponding Ti foil.

Transmission electron microscopy (TEM) was used to analyze the microstructure of the prepared pure TiO_2 nanotubes. Figure 3a shows the TEM images of the pure TiO_2 nanotubes, which were heat-treated at 500 °C for 2 h. The wall thickness of the TiO_2 nanotubes is relatively uniform along the length of the

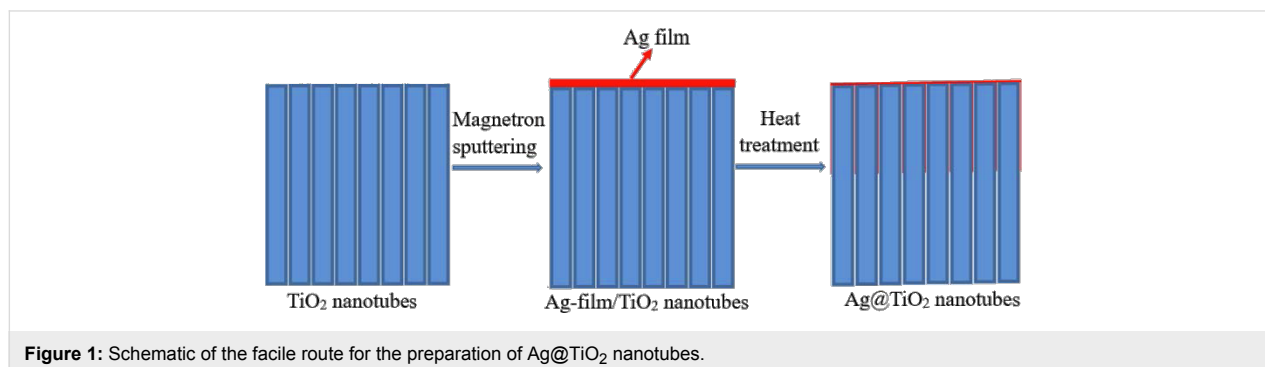


Figure 1: Schematic of the facile route for the preparation of Ag@TiO_2 nanotubes.

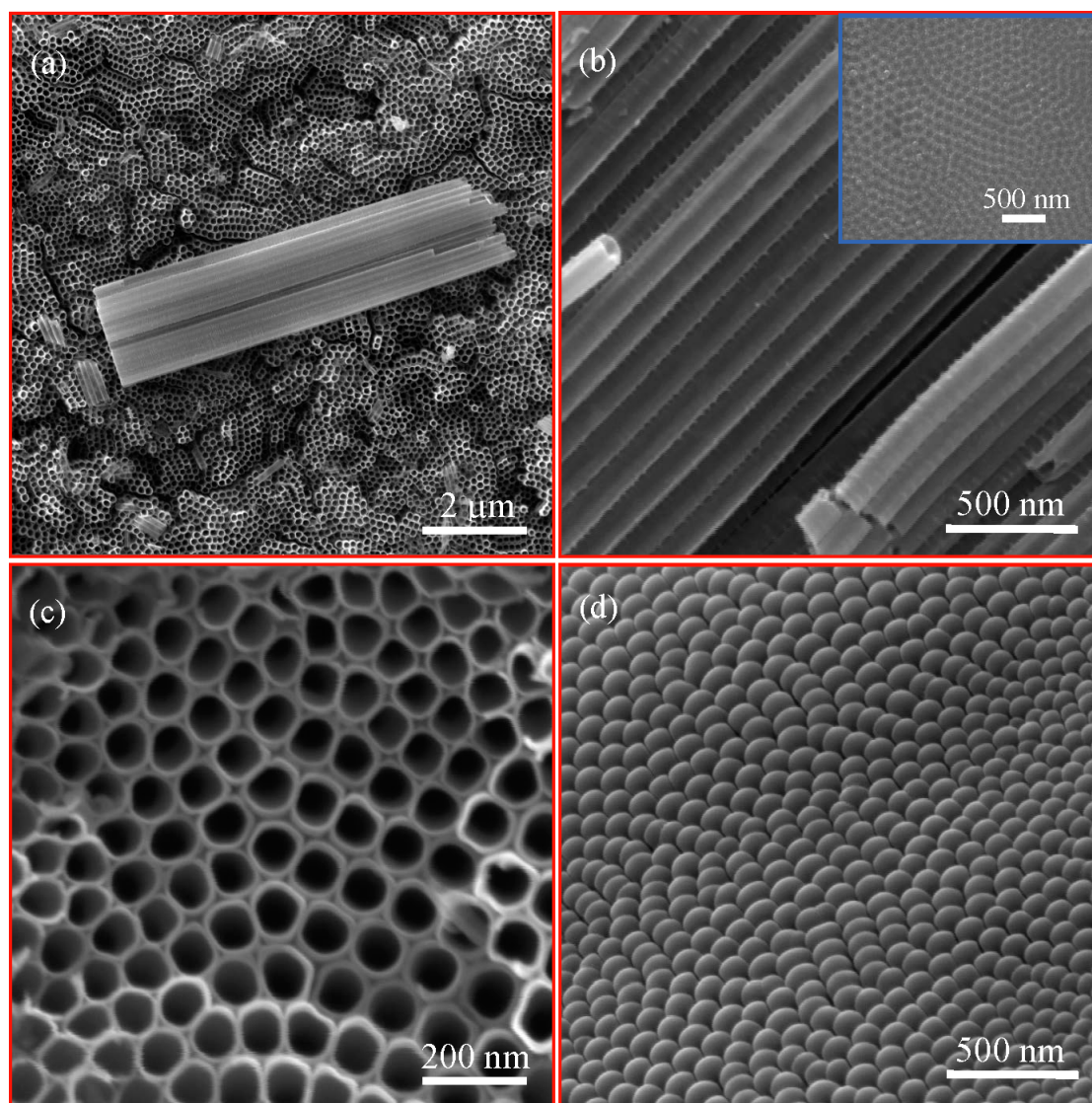


Figure 2: SEM images of the prepared pure TiO₂ nanotubes by a two-step anodization process without heat treatment; (a) overview of the TiO₂ nanotubes with an inserted image showing the average length of about 6.5 μm of the TiO₂ nanotubes, (b) side view of the TiO₂ nanotubes with an inserted image showing well-ordered round imprints on the Ti foil after removing the TiO₂ nanotubes formed by a one-step anodization process, and (c) top view of the TiO₂ nanotubes, and (d) bottom view of the TiO₂ nanotubes.

nanotubes. There is no significant change in the morphology of the pure TiO₂ nanotubes after the heat treatment. The average inner diameter and wall thickness of the pure TiO₂ nanotubes are ca. 75 and ca. 7 nm, respectively, in accord with the SEM observation.

The selective area electron diffraction (SAED) pattern of the pure TiO₂ nanotubes shown in Figure 3b depicts diffraction rings, suggesting the formation of TiO₂ polycrystals after heat treatment. From the HRTEM (high-resolution TEM) analysis shown in Figure 3c, a width of 3.52 Å between neighboring lattice fringes is observed in agreement with the (101) lattice spacing of anatase TiO₂ [30,31]. This result reveals the highly

crystalline nature of the TiO₂ nanotubes in accord with the SAED pattern. The heat treatment can lead to a transition of TiO₂ nanotubes from the amorphous phase to a crystalline phase, which has been observed by Jarose et al. [32].

It must be emphasized that the heat treatment with a temperature less than and equal to 500 °C does not cause any morphological changes of the pure TiO₂ nanotubes, as demonstrated in Figure 2 and Figure 3. The outmost surface of the pure TiO₂ nanotubes remained relatively clean and smooth.

A Ag nanofilm of 230 ± 10 nm in thickness was deposited on top of the prepared pure TiO₂ nanotube arrays. The pure TiO₂

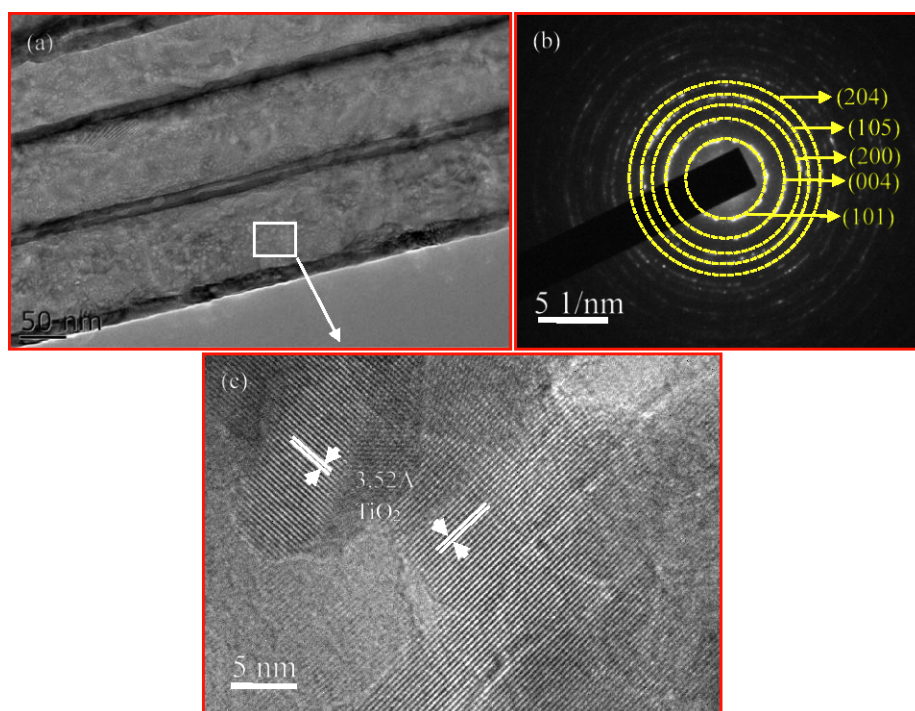


Figure 3: TEM images of the pure TiO_2 nanotubes heat-treated at 500 °C for 2 h; (a) TEM image of the pure TiO_2 nanotubes, (b) SAED pattern showing the presence of TiO_2 nanocrystals, and (c) HRTEM image of a pure TiO_2 nanotube.

nanotube arrays with Ag nanofilm were heat-treated at three temperatures of 300, 400, and 500 °C in air for different periods of time. X-ray diffraction (XRD) was used to analyze the crystal structure of Ti and Ag in the heat-treated TiO_2 nanotube arrays with Ag nanofilm. Figure 4 shows the XRD pattern of the TiO_2 nanotube arrays with Ag nanofilm. No crystallinity of TiO_2 is observable for the untreated TiO_2 nanotube arrays with

Ag nanofilm, and the coating of the Ag nanofilm does not cause any change of the microstructure of the TiO_2 nanotube arrays. The XRD patterns of all the heat-treated TiO_2 nanotube arrays with Ag nanofilm clearly display the peaks of TiO_2 , suggesting the transition of TiO_2 from the amorphous phase to the crystalline phase in accord with the results observed from the TEM analysis. The diffraction peaks with the 2θ values of ca. 25.3°,

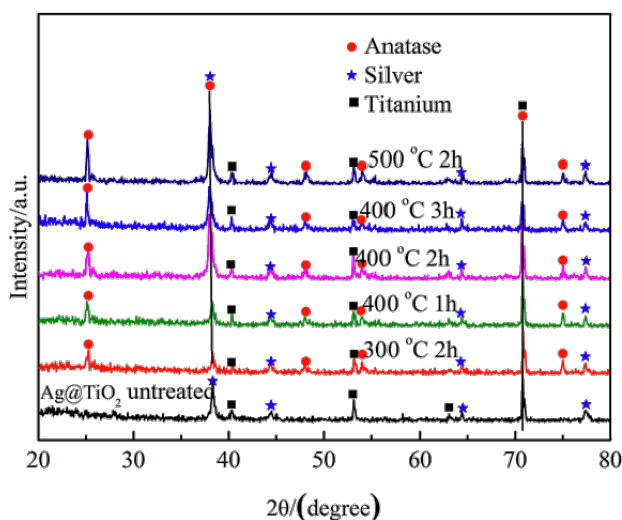


Figure 4: XRD patterns of TiO_2 nanotube arrays with Ag nanofilm heat treated at three different temperatures for different periods of time.

ca. 37.8° , ca. 48.0° , ca. 54.0° and ca. 75.0° shown in Figure 4 correspond to the spacings of the (101), (004), (200), (105), and (215) crystal lattice planes of the anatase phase of TiO_2 in accord with the values in the standard card (JCPDS NO.21-1272). No diffraction peaks for the rutile phase of TiO_2 are detectable. The diffraction peaks with the 2θ values of ca. 38.1° , ca. 44.3° , ca. 64.4° and ca. 77.4° correspond to spacings of the (111), (200), (220) and (311) crystal lattice planes of cubic Ag with a lattice constant of 4.0861 Å (JCPDS NO.65-2871). The diffraction peaks with the 2θ values of ca. 40.2° , ca. 53.0° , ca. 63.0° and ca. 70.7° correspond to the spacings of the (101), (102), (110) and (103) crystal lattice planes of Ti substrate (JCPDS NO.65-6231).

Figure 5 shows SEM images of the TiO_2 nanotube arrays with Ag nanofilm after heat treatment at different temperatures for 2 h. It is evident that a Ag nanofilm of about 225 nm was deposited on the top of the TiO_2 nanotube arrays. Without heat treatment, there is little Ag migrating through the TiO_2 nanotubes, as shown in Figure 5a. The outmost surface of the TiO_2

nanotubes remains relatively clean and smooth. The magnetron sputtering did not cause any significant migration/diffusion of Ag through the TiO_2 nanotube arrays. The Ag nanofilm generally covered the top of the TiO_2 nanotube arrays (see Figure S2a in Supporting Information File 1) and made the topology of the TiO_2 nanotubes indistinguishable. With the heat treatment at 300°C for 2 h, Ag migrated slightly into the TiO_2 nanotube arrays, as shown in Figure 5b. There are Ag nanoparticles present on the outmost surface of the TiO_2 nanotubes. The Ag nanofilm became irregular due to the migration of Ag through the TiO_2 nanotube arrays and dewetting of the Ag nanofilm, and the topology of TiO_2 nanotubes become visible (see Figure S2b in Supporting Information File 1). The increase of the temperature to 400°C for the heat treatment caused a significant amount of Ag to migrate through the TiO_2 nanotube arrays, as shown in Figure 5c, leading to the formation of Ag nanoparticles. There was a layer of Ag over the TiO_2 nanotubes. Ag nanoparticles scattered around the propagation front, likely representing the nucleation and growth of Ag nanoparticles induced by the migration/diffusion of Ag during the heat treat-

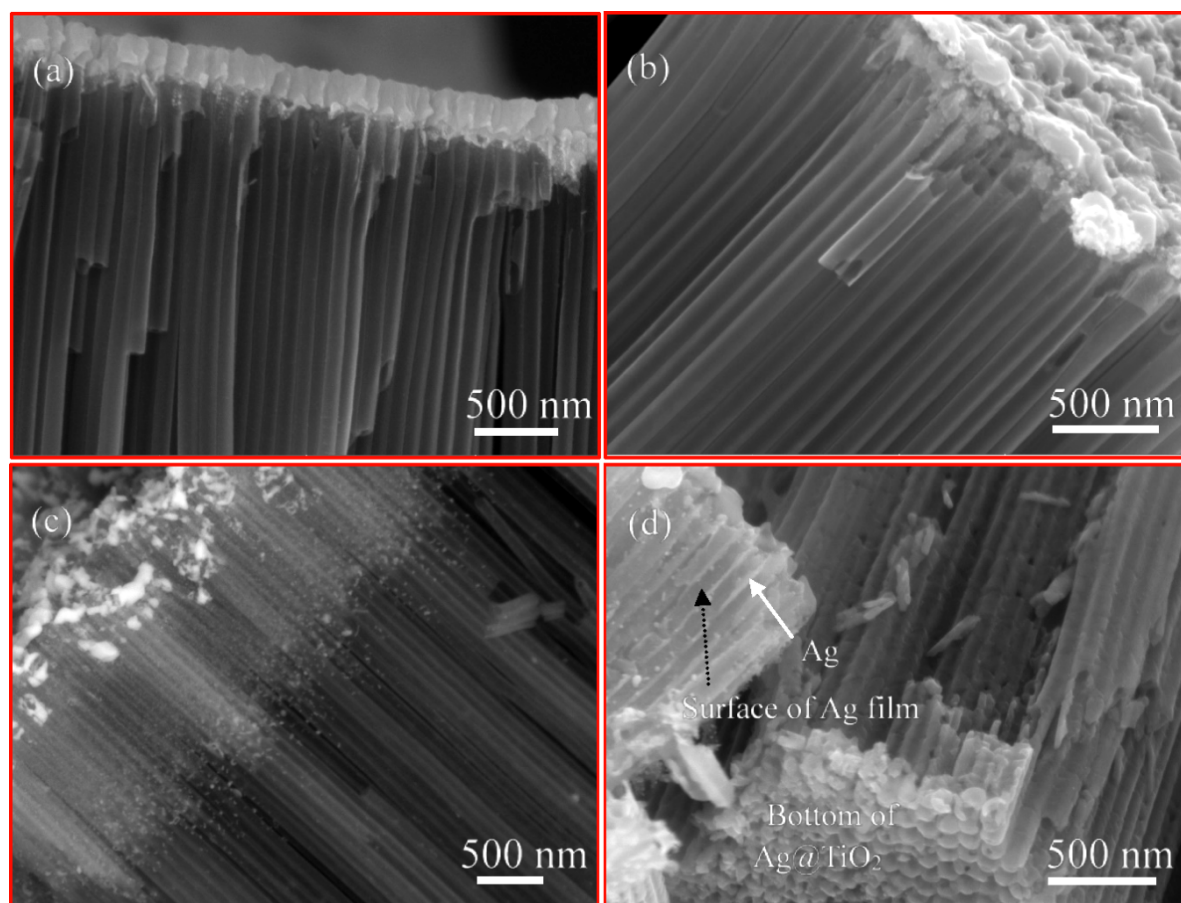


Figure 5: SEM images of the TiO_2 nanotube arrays with Ag nanofilm after different heat treatment for 2 h; (a) without heat treatment, (b) heat treatment at 300°C , (c) heat treatment at 400°C , and (d) heat treatment at 500°C .

ment. For the segment of the TiO_2 nanotubes not covered by the Ag layer and Ag nanoparticles, the outmost surface remained relatively clean and smooth. Figure S3 in Supporting Information File 1 shows the line scan of EDX of the cross section of the corresponding TiO_2 nanotube arrays with Ag nanofilm, which supports the SEM image shown in Figure 5c. Further increase of the temperature to 500 °C for the heat treatment introduced an interesting phenomenon, as shown in Figure 5d. After heat treatment at 500 °C for 2 h, Ag migrated completely through the TiO_2 nanotube arrays to the interface between the TiO_2 nanotubes and the Ti foil and formed a “film” of Ag covering the outmost surface of the TiO_2 nanotubes. The Ag “film” basically occupied the space between TiO_2 nanotubes. Ag atoms migrated through the space between TiO_2 nanotubes instead of migrating/diffusing through the inner surface of the TiO_2 nanotubes. There are probably hardly any Ag nanoparticles formed inside the TiO_2 nanotubes through the migration of Ag, where some Ag nanoparticles are present on the surface of the Ag film. As shown in Figure S2 in Supporting Information File 1, more TiO_2 nanotubes become visible for the heat treatment at higher temperatures, which confirms the migration of

Ag through the TiO_2 nanotube arrays. The increase in the temperature for the heat treatment of the TiO_2 nanotube arrays with Ag nanofilm enhances the migration of Ag atoms, suggesting that the migration of Ag atoms is a thermal activation process.

Figure 6 shows SEM images of the TiO_2 nanotube arrays with Ag nanofilm, which were heat treated at 400 °C for 1, 2, 3 and 4 h. It is evident that the migration/diffusion length of Ag atoms into the TiO_2 nanotube arrays increases with the increase of the heating time, as expected. Relatively uniform migration/diffusion lengths are observed for each individual heating time, even though there are some regions with larger migration/diffusion lengths. A significant amount of Ag nanoparticles near the propagation fronts was formed after all four periods of time.

TEM was used to analyze the microstructures of the heat-treated TiO_2 nanotube arrays with Ag nanofilm. Figure 7 shows the TEM images of the TiO_2 nanotube arrays with Ag nanofilm heat-treated at 500 °C for 2 h. The morphology of TiO_2 nanotubes remained the same except the presence of a layer of Ag nanoparticles, as shown in Figure 7a, which is in accord with

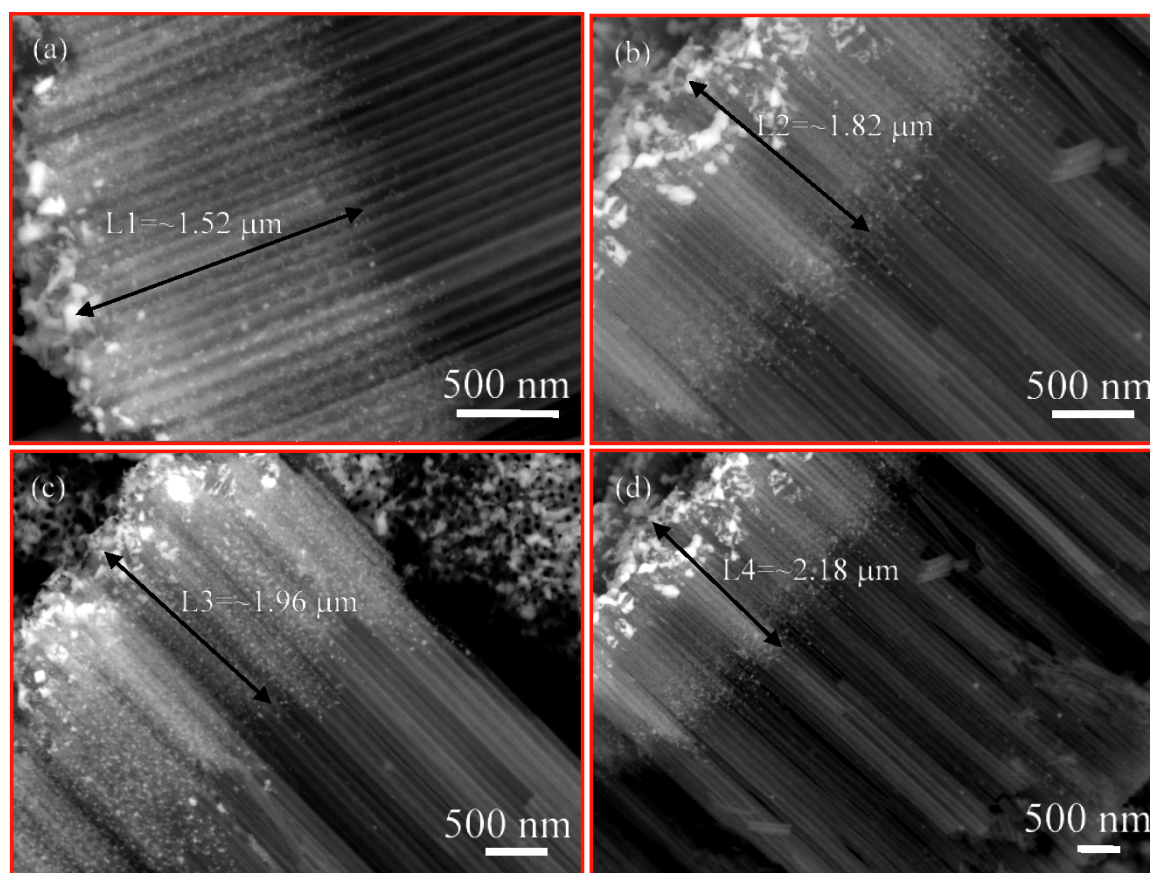


Figure 6: SEM images of the heat-treated TiO_2 nanotube arrays with Ag nanofilm at 400 °C for different periods of time: (a) 1 h, (b) 2 h, (c) 3 h, and (d) 4 h.

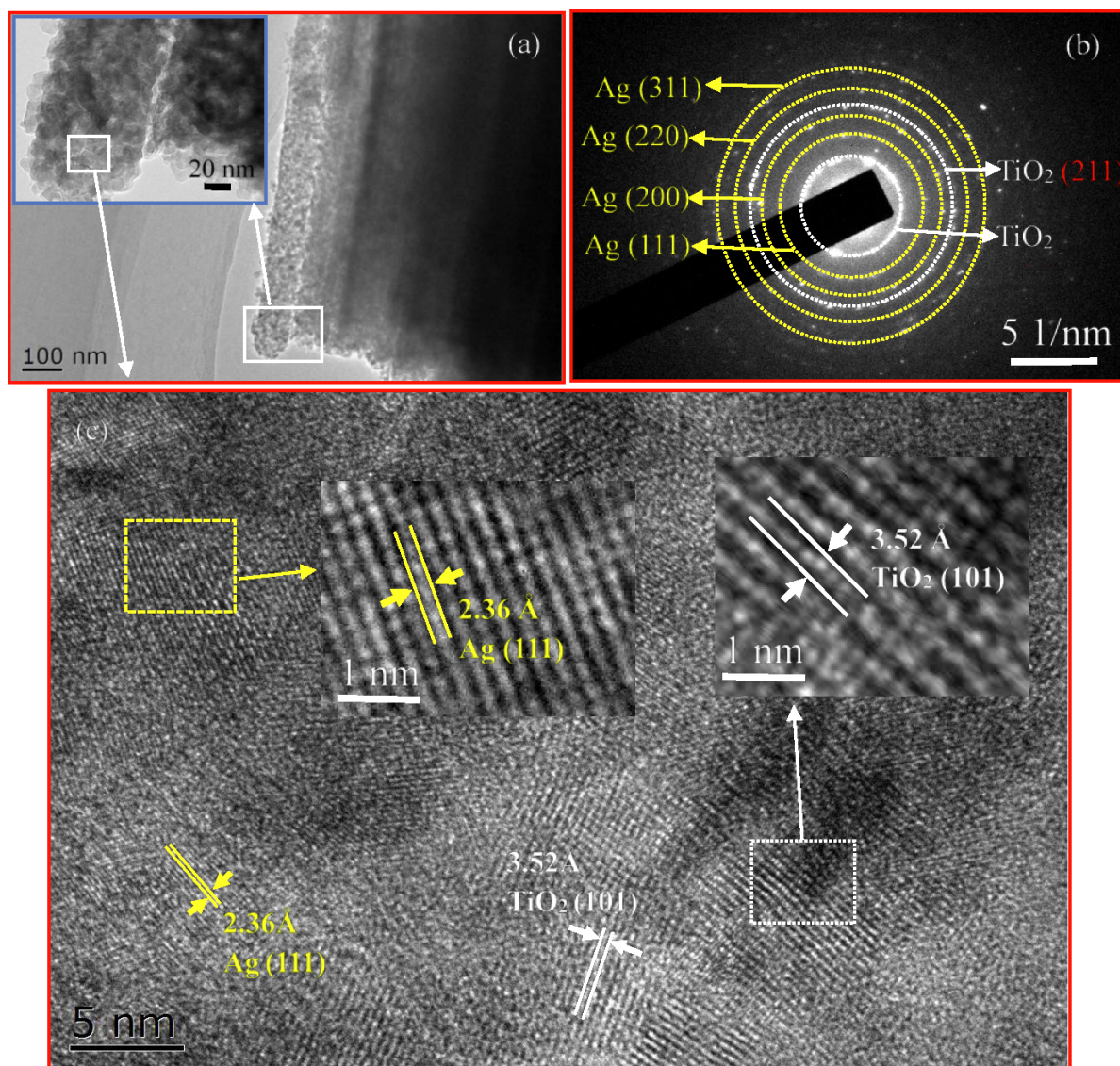


Figure 7: TEM images of the TiO₂ nanotube arrays with Ag nanofilm heat treated at 500 °C for 2 h; (a) TEM image of a TiO₂ nanotube covered by a Ag nanofilm, which consists of numerous Ag nanoparticles, (b) SAED pattern showing the presence of Ag nanocrystals, and (c) HRTEM image of the Ag nanofilm showing characteristic lattice spacings of 3.52 Å for TiO₂ nanotubes and 2.36 Å for Ag.

the images shown in Figure 5 and Figure 6. The migration/diffusion of Ag and heat treatment do not change the nanotubular structure of TiO₂. It is interesting to note that the Ag film, which covers the outmost surface of the TiO₂ nanotubes, is not continuous and made of Ag nanoparticles of about 10 nm in size, as shown in the image embedded in Figure 7a.

The EDS result (see Figure S4 in Supporting Information File 1) reveals the presence of Ti, O, and Ag, confirming the existence of Ag around the TiO₂ nanotubes. The SAED pattern of the Ag film on the outmost surface of TiO₂ nanotubes, as shown in Figure 7b, displays diffuse rings, suggesting that Ag nanoparticles are present in the form of polycrystals. This result

suggests that Ag was not oxidized during the heat treatment. The (111), (200), (220) and (311) crystal planes of cubic Ag are observed, in good accord with the XRD analysis. The HRTEM image shown in Figure 7c depicts the characteristic lattice fringe of 3.52 Å for TiO₂ nanotubes and 2.36 Å for Ag, which correspond to the (101) plane of anatase TiO₂ and {111} planes of face-centered cubic (fcc) structure of Ag [33], respectively. The Ag nanoparticles are Ag nanocrystals. There is no oxidation of Ag nanocrystals in contrast to the general statement that Ag nanoparticles are very reactive and are easily oxidized under the condition of UV irradiation, ambient atmosphere and room temperature [34]. Heat treatment at relatively high temperatures likely leads to the decomposition of silver oxide [34].

It is worth mentioning that the heat-treatment-induced migration/diffusion of Ag into the TiO₂ nanotube arrays of anatase phase has also been observed. The SEM images in Figure S6 in Supporting Information File 1 for the TiO₂ nanotube arrays of anatase phase with Ag film heat treated at 500 °C in air for 2 h demonstrates the presence of Ag nanoparticles on the outmost surface of the TiO₂ nanotube arrays of anatase phase. Ag atoms can migrate into TiO₂ nanotube arrays of either amorphous phase or anatase phase.

Discussion

As shown in Figure 5 and Figure 6, there are probably only very few Ag nanoparticles formed inside the TiO₂ nanotubes through the migration of Ag. Such behavior reveals the curvature effect on the distribution or wetting of Ag on the surface of the TiO₂ nanotubes. According to the Gibbs–Thomson relation [35,36], the equilibrium concentration of solute atoms on a curved surface is determined by the surface energy and the mean curvature. Thus, the equilibrium concentration of Ag atoms on the inner surface of a TiO₂ nanotube is lower than that on the planar surface of TiO₂ of the same structure, and on the outer surface it is higher than that on the planar surface. Ag atoms are preferred to migrate on the outmost surface of the TiO₂ nanotubes and form a layer of Ag during the heat treatment, as observed in Figure 5 and Figure 6.

According to the theory of thermodynamics [37], the melting point of a material is a function of the size of the material. The size dependence of the melting point of a material in spherical shape can be expressed as [38]

$$T_m(r) = T_m(\infty) \exp\left(\frac{\alpha - 1}{1 - r/r_0}\right), \quad (1)$$

with

$$\alpha = \frac{2S_{\text{vib}}(\infty)}{3R} + 1 \quad \text{and} \quad r_0 = (3 - d)h. \quad (2)$$

Here, $T_m(r)$ is the melting temperature of the material in a spherical shape of radius r , $T_m(\infty)$ is the melting temperature of the material in bulk shape, R is the gas constant, $S_{\text{vib}}(\infty)$ is the vibrational melting entropy of the material, h is the atomic radius of the material, and $d = 0$ for nanoparticles. As shown in Figure S7 of Supporting Information File 1, the radius of Ag nanoparticles is in the range from 2.6 ± 0.2 to 5 ± 2 nm. From Equation 1 and Equation 2, one can note that the smaller the size of nanoparticle, the lower is the melting point. Using the parameters of $h = 0.2898$ nm [39], $T_m(\infty) = 1234$ K [40], $S_{\text{vib}}(\infty) = 7.98$ J mol^{−1}·K^{−1} [38] in Equation 1, one obtains a

melting temperature of 857.5 K (584.5 °C) for the smallest size of Ag crystalline nanoparticles (2.4 nm), which is much higher than 300–500 °C used in the heat treatment. The formation of Ag nanocrystals on the outmost surface of the TiO₂ nanotubes involves the nucleation and growth processes controlled by the migration/diffusion of Ag atoms.

Generally, the migration of Ag through the TiO₂ nanotube arrays involves diffusion, which is controlled by the gradient of concentration. With the deposition of a Ag film on the top of highly ordered TiO₂ nanotube arrays, the diffusion of Ag on the outmost surface of the TiO₂ nanotubes can be approximated as a one-dimensional problem. The equation describing the diffusion of Ag along the outmost surface of the TiO₂ nanotubes is

$$\frac{\partial c}{\partial t} = D \frac{\partial^2 c}{\partial x^2}. \quad (3)$$

Here, c is an average concentration of Ag over the cross-sectional area confined by three adjacent TiO₂ nanotubes that are in contact with each other. The condition of zero flux in the direction normal to the outmost surface was used to derive Equation 3. The concentration at the top of the TiO₂ nanotubes can be approximated as constant, i.e.,

$$c(0, t) = c_0. \quad (4)$$

Here, c is the concentration of Ag atoms, c_0 is the concentration of Ag atoms at the top of the TiO₂ nanotubes, t is the time, D is the diffusivity of Ag atoms, and x is the migration distance of Ag on the outmost surface of the TiO₂ nanotubes. The initial condition is

$$c(x, t) = 0. \quad (5)$$

The solution of Equations 3–5 can be found as

$$c(x, t) = c_0 \left(1 - \frac{2}{\sqrt{\pi}} \int_0^{x/2\sqrt{Dt}} e^{-\xi^2} d\xi \right). \quad (6)$$

For $c(x, t)/c_0 = 0.01$, one obtains

$$x = 3.64\sqrt{Dt}, \quad (7)$$

which shows that the migration distance of Ag atoms on the outmost surface of the TiO₂ nanotubes is proportional to the square root of time, as expected for random diffusion. Using the SEM images shown in Figure 6, the temporal variation of the

migration distance of Ag atoms on the outmost surface of the TiO₂ nanotubes for the heat treatment at 400 °C is depicted in Figure 8. It is evident that there is a linear relation between the square root of the migration time and the migration distance of Ag atoms on the outmost surface of the TiO₂ nanotubes, which is in accord with Equation 7. Using the linear regression to fit the experimental data in Figure 8, one obtains the diffusivity of $6.87 \times 10^{-18} \text{ m}^2/\text{s}$.

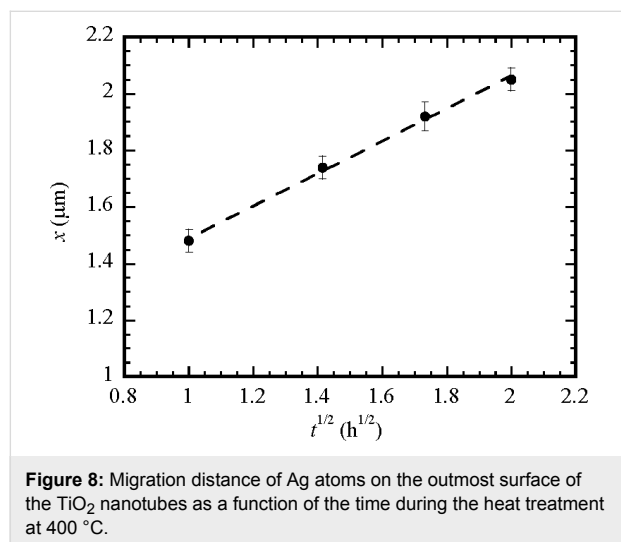


Figure 8: Migration distance of Ag atoms on the outmost surface of the TiO₂ nanotubes as a function of the time during the heat treatment at 400 °C.

It is known that the temperature dependence of diffusivity follows an Arrhenius relation as $D = D_0 \cdot \exp(-Q/RT)$ with D_0 being a pre-exponential constant, Q is the activation energy for the rate process, R is the gas constant, and T is the absolute temperature. Using the Arrhenius relation, the temperature dependence of the migration distance of Ag on the outmost surface of the TiO₂ nanotubes during the heat treatment can be expressed as

$$x = 3.64 \sqrt{D_0 t} e^{-Q/2RT} \quad (8)$$

As shown in Figure 5d, Ag migrated completely through the TiO₂ nanotube arrays to the interface between the TiO₂ nano-

tubes and the Ti foil during the heat treatment at 500 °C for 2 h. One can approximate the migration distance of Ag atoms on the outmost surface of the TiO₂ nanotubes as about 6.5 μm of the length of the TiO₂ nanotubes for the heat treatment at 500 °C for 2 h. Figure 9 shows the temperature dependence of the migration distance of Ag atoms on the outmost surface of the TiO₂ nanotubes for a heat treatment of 2 h. Using Equation 8 to fit the experimental data shown in Figure 9, one obtains the activation energy of 157 kJ/mol for the migration/diffusion of Ag atoms on the outmost surface of the TiO₂ nanotubes in the temperature range of 300 to 500 °C.

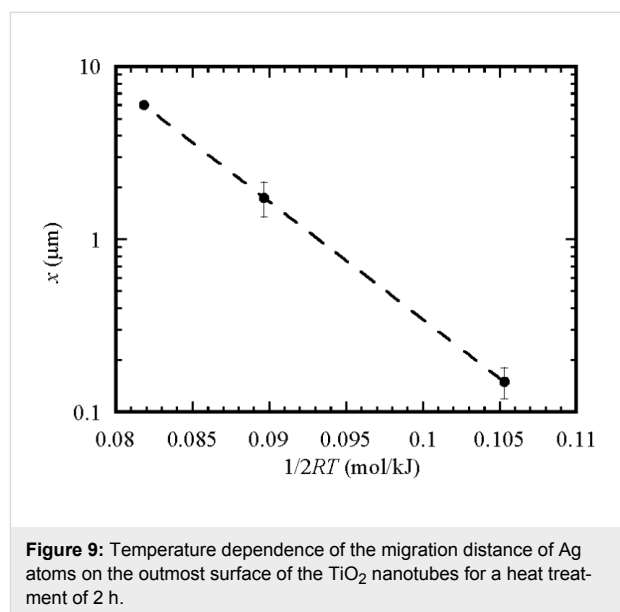


Figure 9: Temperature dependence of the migration distance of Ag atoms on the outmost surface of the TiO₂ nanotubes for a heat treatment of 2 h.

There are studies on the diffusion of Ag, including self-diffusion, grain boundary diffusion, and diffusion of Ag in amorphous TiO₂ films. Table 1 summarises the data available in literature for the diffusivity and activation energy of the diffusion of Ag. For comparison, the results obtained in this work are also included in Table 1. It is evident that the diffusivity of Ag on the outmost surface of the TiO₂ nanotubes is three orders of magnitude larger than the results reported by Kulczyk-Malecka et al. [41] for the sandwich structure of TiO₂/Ag/TiO₂ coatings,

Table 1: Diffusivity and activation energy for the diffusion of Ag.

	temperature (°C)	diffusivity (m ² /s)	activation energy (kJ/mol)
diffusion of Ag in TiO ₂ /Ag/TiO ₂ coatings [41]	100–400	$(3.5\text{--}5.8) \times 10^{-21}$	127.5
diffusion of Ag in TiO ₂ /Ag/TiO ₂ coatings [41]	600	5.93×10^{-20}	3.5
lattice diffusion of Ag [42]	400	1.1×10^{-19}	192.0
grain boundary diffusion of Ag [42]	400	6.0×10^{-18}	111
Ag diffusion into Au core [43]	27	$(7.5\text{--}21) \times 10^{-25}$	
Ag on surface of TiO ₂ nanotubes (this work)	400	6.87×10^{-18}	157

and the activation energy is also larger than that given by Kulczyk-Malecka et al. [41]. Such differences reveal the effect of the microstructure on the diffusion behavior of Ag. The TiO₂ in TiO₂/Ag/TiO₂ coatings was present in the form of thin film and amorphous phase. Also, the time of the heat treatment for the measurement of the diffusivity was 5 min [41], which is much less than the time used in this work. It is interesting to note that the diffusivity obtained in this work is compatible with the diffusivity for the grain boundary diffusion of Ag with the activation energy being less than that for the lattice diffusion of Ag and larger than that for the grain boundary diffusion. Such a result suggests that both the grain boundary diffusion of Ag and the interface diffusion on the surface of the TiO₂ nanotubes play important roles in controlling the migration/diffusion of Ag into the TiO₂ nanotube arrays.

Conclusion

In summary, an approach has been developed to coat the outmost surface of TiO₂ nanotubes in nanotube arrays with Ag via the deposition of Ag films on top of the TiO₂ nanotube arrays by magnetron sputtering and subsequent heat treatment at a temperature between 300 and 500 °C. A two-step anodization process was used to prepare the TiO₂ nanotube arrays. The migration of Ag atoms through the TiO₂ nanotube arrays was investigated ex situ by using SEM and TEM. In contrast to the Ag@TiO₂ nanotubes prepared by the methods involving aqueous solutions, Ag nanocrystals were formed on the outmost surface of TiO₂ nanotubes. There probably were hardly any Ag nanocrystals formed inside the TiO₂ nanotubes through the migration of Ag. Such a result reveals that Ag atoms prefer to migrate/diffuse on the convex surface of the TiO₂ nanotubes. The average migration/diffusion length of Ag atoms on the outmost surface of the TiO₂ nanotubes along the longitudinal direction of the TiO₂ nanotubes increases with the increase of the heat treatment temperature and the heating time. During the heat treatment at 500 °C for 2 h, Ag atoms migrated completely through the TiO₂ nanotube arrays and formed an Ag nanofilm, which consists of numerous Ag nanocrystals, covering the outmost surface of the TiO₂ nanotubes.

Using the theory of diffusion, the migration/diffusion of Ag atoms on the outmost surface of the TiO₂ nanotubes was analyzed. The diffusivity for the diffusion of Ag atoms on the outmost surface of the TiO₂ nanotubes at 400 °C is $6.87 \times 10^{-18} \text{ m}^2/\text{s}$, which is three orders of magnitude larger than the results reported by Kulczyk-Malecka et al. [41] for the sandwich structure of TiO₂/Ag/TiO₂ coatings. Such a result demonstrates the fast diffusion of Ag atoms on the surface of the TiO₂ nanotubes. The activation energy for the migration/diffusion of Ag on the outmost surface of the TiO₂ nanotubes in the temperature range of 300 to 500 °C is 157 kJ/mol, which is

less than that for the lattice diffusion of Ag and larger than that for the grain boundary diffusion. Both the grain boundary diffusion of Ag and the interface diffusion on the outmost surface of the TiO₂ nanotubes play important roles in the migration/diffusion of Ag into the TiO₂ nanotube arrays.

Experimental

Preparation of TiO₂ nanotubes

TiO₂ nanotubes on Ti foils (99.9 atom %) were fabricated via a two-step anodization process [44]. Briefly, commercially available pure titanium foils ($30 \times 10 \times 0.1 \text{ mm}^3$, China Research Institute of Nonferrous Metals, China) were ultrasonically cleaned with acetone, ethanol, and deionized water for 15 min each. Anodization of the Ti foils was performed in a mixture of water, ethylene glycol and 0.13 M NH₄F, using a conventional two-electrode cell system. The volume ratio of water to ethylene glycol was 2:100. The cleaned Ti foil was used as the working electrode, and a platinum foil was used as the counter electrode. The anodization voltage was 50 V, and the anodization time was 1 h. TiO₂ nanotubes with “bamboo-like” structure at the outer layer were obtained (Figure S1c in Supporting Information File 1). The TiO₂ nanotubes with “bamboo-like” structure were completely removed ultrasonically from the as-anodized Ti foils, resulting in well-ordered round imprints on the surface of the Ti foils (see the inserted image in Figure 2b). After being cleaned ultrasonically, the Ti foils were anodized for another 30 min under the same condition to obtain the two-step TiO₂ nanotube arrays with relatively clean outmost surface (Figure 2b). The prepared TiO₂ nanotube arrays were rinsed with water and dried in air.

Deposition of Ag nanofilms on the top of TiO₂ nanotube arrays

Ag nanofilm of $230 \pm 10 \text{ nm}$ in thickness was deposited on the top of the TiO₂ nanotube arrays at room temperature (25 °C) via magnetron sputtering in a multifunctional magnetron sputtering instrument (JGP560B), using an Ag target. Argon gas was flowed into the sputtering chamber after the pressure of the sputtering chamber reached $8 \times 10^{-4} \text{ Pa}$. The surface residuals were removed via pre-sputtering. During the sputtering, argon gas flowed through the chamber at a rate of 30 sccm and a chamber pressure of 6 Pa. The separation between the top of the TiO₂ nanotubes and the target was about 30 mm.

The TiO₂ nanotube arrays with Ag nanofilms were heat treated at temperatures of 300, 400 and 500 °C, respectively, for different holding times (1, 2 and 3 h) at a ramping rate of $2 \text{ °C} \cdot \text{min}^{-1}$ in a tube furnace in air. The heat treatment allowed Ag to migrate through the TiO₂ nanotubes. Figure 1 shows schematically the facile route for the preparation of Ag@TiO₂ nanotubes.

Materials characterization

The morphology and selected area electron diffraction (SAED) patterns of the prepared structures were examined using field-emission scanning electron microscopy (FESEM) (Tescan MIRA3 LMH) at 10 kV and transmission electron microscopy (TEM) (JEOL 2100-F) at 200 kV. The composition of the prepared structures was determined using energy dispersive spectroscopy (EDS) (OXFORD X-Max 80), and the crystal structure of the prepared structures was analyzed with Cu K α radiation on a Rigaku D/max 2500 X-ray diffractometer with patterns recorded in a range of 20–80°.

To prepare the TEM specimens, the as-prepared Ag@TiO₂ nanotubes, which were scratched from the Ag@TiO₂ nanotube arrays using a pair of sharp tweezers, were treated ultrasonically in ethanol for 5–8 min to form a suspension. A drop of the suspension was then dripped on a carbon film supported by a copper grid and dried in air before the TEM analysis.

Supporting Information

Supporting Information File 1

Additional experimental results.

[<http://www.beilstein-journals.org/bjnano/content/supplementary/2190-4286-7-105-S1.pdf>]

Acknowledgements

LW is grateful for the financial support from the National Natural Science Foundation of China (51301118, 51274149) and the Scientific and Technological Innovation Programs of Higher Education Institutions in Shanxi province (2013108). WGZ is grateful for the support from China Scholarship Council and the Fundamental Research Funds for the Central Universities. FY is grateful for the support from the “Hundred-People-Plan” Program of Shanxi (2014). LYM is grateful for the support from Natural Science Foundation of Shanxi province (2015021066).

References

- Kim, M. S.; Lee, T.-W.; Parka, J. H. *J. Electrochem. Soc.* **2009**, *156*, A584–A588. doi:10.1149/1.3129682
- Deng, D.; Kim, M. G.; Lee, J. Y.; Cho, J. *Energy Environ. Sci.* **2009**, *2*, 818–837. doi:10.1039/b823474d
- Zeng, P.; Liu, Z.; Hu, Z.; Zhai, J.; Jiang, L. *RSC Adv.* **2013**, *3*, 22853–22856. doi:10.1039/c3ra43906b
- Zhao, B. T.; Jiang, S. M.; Su, C.; Cai, R.; Ran, R.; Tadé, M. O.; Shao, Z. *J. Mater. Chem. A* **2013**, *1*, 12310–12320. doi:10.1039/c3ta12770b
- Weng, Z.; Guo, H.; Liu, X.; Wu, S.; Yeung, K. W. K.; Chu, P. K. *RSC Adv.* **2013**, *3*, 24758–24775. doi:10.1039/c3ra44031a
- Hemalatha, K.; Prakash, A. S.; Guruprakash, K.; Jayakumar, M. *J. Mater. Chem. A* **2014**, *2*, 1757–1766. doi:10.1039/C3TA13352D
- Lee, E. J.; Nam, I.; Yi, J.; Bang, J. H. *J. Mater. Chem. A* **2015**, *3*, 3500–3510. doi:10.1039/C4TA05988C
- Wu, Q. L.; Li, J.; Deshpande, R. D.; Subramanian, N.; Rankin, S. E.; Yang, F.; Cheng, Y.-T. *J. Phys. Chem. C* **2012**, *116*, 18669–18677. doi:10.1021/jp3072266
- Zhang, W.; Liu, Y.; Zhou, D.; Wen, J.; Liang, W.; Yang, F. *RSC Adv.* **2015**, *5*, 57155–57163. doi:10.1039/C5RA08802J
- Kraeutler, B.; Bard, A. J. *J. Am. Chem. Soc.* **1977**, *99*, 7729–7731. doi:10.1021/ja00465a065
- Nakato, Y.; Tsumura, A.; Tsubomura, H. *J. Phys. Chem.* **1983**, *87*, 2402–2405. doi:10.1021/j100236a032
- Nakato, Y.; Akanuma, H.; Shimizu, J.-i.; Magari, Y. *J. Electroanal. Chem.* **1995**, *396*, 35–39. doi:10.1016/0022-0728(95)04007-B
- Bauer, R.; Waldner, G.; Fallmann, H.; Hager, S.; Klare, M.; Krutzler, T.; Malato, S.; Maletzky, P. *Catal. Today* **1999**, *53*, 131–144. doi:10.1016/S0920-5861(99)00108-X
- Ma, D.; Yan, Y.; Ji, H.; Chen, C.; Zhao, J. *Chem. Commun.* **2015**, *51*, 17451–17454. doi:10.1039/C5CC07123B
- Linsebigler, A. L.; Lu, G.; Yates, J. T., Jr. *Chem. Rev.* **1995**, *95*, 735–758. doi:10.1021/cr00035a013
- Shankar, K.; Basham, J. I.; Allam, N. K.; Varghese, O. K.; Mor, G. K.; Feng, X. J.; Paulose, M.; Seabold, J. A.; Choi, K.-S.; Grimes, C. A. *J. Phys. Chem. C* **2009**, *113*, 6327–6359. doi:10.1021/jp809385x
- Rolison, D. R. *Science* **2003**, *299*, 1698–1701. doi:10.1126/science.1082332
- Tang, H.; Lévy, F.; Berger, H.; Schmid, P. E. *Phys. Rev. B* **1995**, *52*, 7771–7774. doi:10.1103/PhysRevB.52.7771
- Pascual, J.; Camassel, J.; Mathieu, H. *Phys. Rev. B* **1978**, *18*, 5606–5614. doi:10.1103/PhysRevB.18.5606
- Amtout, A.; Leonelli, R. *Phys. Rev. B* **1995**, *51*, 6842–6851. doi:10.1103/PhysRevB.51.6842
- Huang, L.; Peng, F.; Wang, H.; Yu, H.; Geng, W.; Yang, J.; Zhang, S.; Zhao, H. *Mater. Chem. Phys.* **2011**, *130*, 316–322. doi:10.1016/j.matchemphys.2011.06.052
- Guo, G.; Yu, B.; Yu, P.; Chen, X. *Talanta* **2009**, *79*, 570–575. doi:10.1016/j.talanta.2009.04.036
- Yan, J.; Song, H.; Yang, S.; Yan, J.; Chen, X. *Electrochim. Acta* **2008**, *53*, 6351–6355. doi:10.1016/j.electacta.2008.04.048
- Amin, S. A.; Pazouki, M.; Hosseinnia, A. *Powder Technol.* **2009**, *196*, 241–245. doi:10.1016/j.powtec.2009.07.021
- Enachi, M.; Guix, M.; Braniste, T.; Postolache, V.; Ciobanu, V.; Ursaki, V.; Schmidt, O. G.; Tiginyanu, I. *Surf. Eng. Appl. Electrochem.* **2015**, *51*, 3–8. doi:10.3103/S1068375515010044
- He, B.-L.; Dong, B.; Li, H.-L. *Electrochem. Commun.* **2007**, *9*, 425–430. doi:10.1016/j.elecom.2006.10.008
- Nam, S. H.; Shim, H.-S.; Kim, Y.-S.; Dar, M. A.; Kim, J. G.; Kim, W. B. *ACS Appl. Mater. Interfaces* **2010**, *2*, 2046–2052. doi:10.1021/am100319u
- Wei, W.; Oltean, G.; Tai, C.-W.; Edström, K.; Björefors, F.; Nyholm, L. *J. Mater. Chem. A* **2013**, *1*, 8160–8169. doi:10.1039/c3ta11273j
- Zhu, K.; Wang, Q.; Kim, J.-H.; Pesaran, A. A.; Frank, A. J. *J. Phys. Chem. C* **2012**, *116*, 11895–11899. doi:10.1021/jp301884x
- Liu, E.; Kang, L.; Wu, F.; Sun, T.; Hu, X.; Yang, Y.; Liu, H.; Fan, J. *Plasmonics* **2014**, *9*, 61–70. doi:10.1007/s11468-013-9598-7
- Xiao, F. *J. Phys. Chem. C* **2012**, *116*, 16487–16498. doi:10.1021/jp3034984

32. Jarosz, M.; Syrek, K.; Kapusta-Kołodziej, J.; Mech, J.; Malek, K.; Hnida, K.; Łojewski, T.; Jaskuła, M.; Sulka, G. D. *J. Phys. Chem. C* **2015**, *119*, 24182–24191. doi:10.1021/acs.jpcc.5b08403
33. Yang, D.; Sun, Y.; Tong, Z.; Tian, Y.; Li, Y.; Jiang, Z. *J. Phys. Chem. C* **2015**, *119*, 5827–5835. doi:10.1021/jp511948p
34. Shpak, A. P.; Gorbik, P. P., Eds. *Nanomaterials and Supramolecular Structures – Physics, Chemistry, and Applications*; Springer: Dordrecht, Netherlands, 2010. doi:10.1007/978-90-481-2309-4
35. Yang, F. *Thin Solid Films* **2004**, *446*, 313–317. doi:10.1016/j.tsf.2003.10.021
36. Gusak, A. M.; Lyashenko, Y. A.; Kornienko, S. V.; Pasichnyy, M. O.; Shirinyan, A. S.; Zaporozhets, T. V., Eds. *Diffusion-controlled solid state reactions: in alloys, thin-films, and nanosystems*; John Wiley & Sons: New York, NY, U.S.A., 2010. doi:10.1002/9783527631025
37. Ragone, D. V. *Thermodynamics of materials*; Wiley: Hoboken, NJ, U.S.A., 1995.
38. Jiang, Q.; Zhang, S.; Zhao, M. *Mater. Chem. Phys.* **2003**, *82*, 225–227. doi:10.1016/S0254-0584(03)00201-3
39. King, H. W. In *Physical Metallurgy*, 3rd ed.; Cahn, R. W.; Haasen, P., Eds.; North Holland: Amsterdam, Netherlands, 1983; p 63.
40. Sargent, W. *Table of periodic properties of the elements*; Sargent-Welch Scientific: Skokie, IL, U.S.A., 1980.
41. Kulczyk-Malecka, J.; Kelly, P. J.; West, G.; Clarke, G. C. B.; Ridealgh, J. A.; Almqvist, K. P.; Greer, A. L.; Barber, Z. H. *Acta Mater.* **2014**, *66*, 396–404. doi:10.1016/j.actamat.2013.11.030
42. Mitchell, B. S. *An introduction to materials engineering and science for chemical and materials engineers*; John Wiley & Sons: New York, NY, U.S.A., 2004.
43. Jiang, Q.; Zhang, S. H.; Li, J. C. *Solid State Commun.* **2004**, *130*, 581–584. doi:10.1016/j.ssc.2004.03.033
44. Yang, Y.; Wang, X.; Li, L. *Mater. Sci. Eng., B* **2008**, *149*, 58–62. doi:10.1016/j.mseb.2007.12.006

License and Terms

This is an Open Access article under the terms of the Creative Commons Attribution License (<http://creativecommons.org/licenses/by/2.0>), which permits unrestricted use, distribution, and reproduction in any medium, provided the original work is properly cited.

The license is subject to the *Beilstein Journal of Nanotechnology* terms and conditions: (<http://www.beilstein-journals.org/bjnano>)

The definitive version of this article is the electronic one which can be found at:
[doi:10.3762/bjnano.7.105](https://doi.org/10.3762/bjnano.7.105)